Research Square

Preprints are preliminary reports that have not undergone peer review.
They should not be considered conclusive, used to inform clinical practice,
or referenced by the media as validated information.

A Practical Inverse Design Approach for High-Entropy Catalysts with Generative AI

Jun Jiang

jiangj1@ustc.edu.cn

University of Science and Technology of China https://orcid.org/0000-0002-6116-5605

Donglai Zhou

University of Science and Technology of China

Ruyu Yang

Hefei National Research Center for Physical Sciences at the Microscale, School of Chemistry and Materials Science, University of Science and Technology of China

Zijin Jia

Key Laboratory of Precision and Intelligent Chemistry, Hefei National Research Center for Physical Sciences at the Microscale, University of Science and Technology of China

Yuhai Cai

Key Laboratory of Precision and Intelligent Chemistry, Hefei National Research Center for Physical Sciences at the Microscale, University of Science and Technology of China

Luyuan Zhao

Hefei National Research Center for Physical Sciences at the Microscale, School of Chemistry and Materials Science, University of Science and Technology of China

Lulu Guo

Key Laboratory of Precision and Intelligent Chemistry, Hefei National Research Center for Physical Sciences at the Microscale, University of Science and Technology of China

Guilin Ye

Key Laboratory of Precision and Intelligent Chemistry, Hefei National Research Center for Physical Sciences at the Microscale, University of Science and Technology of China

Song Wang

University of Science and Technology of China https://orcid.org/0000-0003-1252-8091

Linjiang Chen

University of Science and Technology of China

Daobin Liu

Key Laboratory of Precision and Intelligent Chemistry, Hefei National Research Center for Physical Sciences at the Microscale, University of Science and Technology of China

Pieter E. S. Smith

Hefei JiShu Quantum Technology Co., Ltd., Hefei 230026, China

Yan Huang
University of Science and Technology of China https://orcid.org/0000-0003-2512-2509
Qing Zhu
Hefei National Research Center for Physical Sciences at the Microscale, School of Chemistry and Materials Science, University of Science and Technology of China https://orcid.org/0000-0003-4278-4205

Article

Keywords:

Posted Date: January 14th, 2025

DOI: https://doi.org/10.21203/rs.3.rs-5712388/v1

License: This work is licensed under a Creative Commons Attribution 4.0 International License.
Read Full License

Additional Declarations: There is **NO** Competing Interest.

Version of Record: A version of this preprint was published at Nature Synthesis on January 29th, 2026. See the published version at https://doi.org/10.1038/s44160-025-00983-5.

Abstract

The vast compositional space of high-entropy materials offers unprecedented opportunities for the development of powerful catalysts. However, their inverse design remains unfeasible due to the lack of robust theoretical frameworks and high-throughput experimental tools. This study demonstrates a practical inverse design approach that integrates spectroscopic descriptors, generative machine learning, and a robotic experimental platform to synthesize and optimize catalyst composition for the oxygen evolution reaction (OER). The automated system significantly accelerated catalysts design and experimental validation, reducing the time required for synthesis, characterization and performance testing from approximately 20 hours to only 78 minutes per sample. Following a rapid screen for efficient senary high-entropy catalysts, the spectroscopic generative model further optimized the top-performing candidate, lowering its overpotential at 10 mA/cm^2 by an additional 32 mV. Our findings are a testament to the potential of an inverse design approach that incorporates spectroscopic descriptors into generative machine learning to accelerate catalyst discovery. Moreover, this approach is also expected to drive the intelligent design of high-performance complex materials.

Introduction

The inverse design of complex materials has remained elusive due to their nearly infinite chemical compositions and their intricate composition-structure-performance relationships.[1–4] This challenge is particularly pronounced for high-entropy catalysts, where the unpredictable nature of the interfacial evolution processes involved in catalytic reactions further complicates the design process.[5–7] Central to this issue is the task of deriving high-dimensional microscopic compositions from low-dimensional performance data. While some progress has been made by carrying out additional theoretical calculations or using experimental data to bridge the dimensionality gap,[8–10] the problem remains unresolved. Precise control over multiple synthetic parameters is typically required, adding another layer of complexity to the inverse design problem. Moreover, because traditional forward trial-and-error design methods rapidly become intractable when confronted with the vast chemical spaces of high-entropy catalysts,[11–13] there remains an urgent need for a paradigm shift in these materials' design.[14–16]

Recently, artificial intelligence-generated content (AIGC) has been employed to efficiently explore vast chemical spaces, propelling the development of catalyst inverse design methodologies.[1,17,18] These approaches often utilize abstract, high-dimensional data representations to generate material with the desired characteristics.[19–23] Variational autoencoders (VAEs), for instance, are powerful generative models that have been extensively used to navigate the optimal chemical combinations to facilitate functional material design.[21,24–26] Descriptors directly capturing system properties are complementary to the aforementioned AIGC approaches. Notably, spectroscopic descriptors compress rich physical information like system geometry and electronic structure, which shows great potential in assisting catalyst development.[27–29] These descriptors can therefore be embedded into the generative models along with machine learning (ML) algorithms for extracting key spectral features, thus establishing a

reliable correlation between spectroscopic signatures and catalytic performance and synthetic composition.[30–32] This inverse design strategy overcomes the limitations of traditional ML models that rely on structural descriptors and therefore struggle to predict the high-dimensional correlations between synthesis, structure, and performance.[33–35]

Building robust ML models necessitates access to large, high-quality datasets.[36–38] The advent of high-throughput, automated experimental platforms has made such comprehensive datasets more accessible, offering significant improvements over traditional manual laboratory operations.[39–42] By integrating intelligent models with synthetic robots, we can overcome many of the obstacles that have traditionally hindered alignment between theoretical prediction and real-world chemical synthesis. Spectroscopic descriptors, in particular, play a critical role in achieving autonomous "closed-loop" materials design. This approach involves feedback between theory and experiment, facilitating the digital inversion from desired properties to structures, unraveling complex relationships between synthetic variables and catalytic reactivity, and providing data- and AI-powered insights for catalyst optimization.

In this proof-of-concept study, we synthesize and optimize high-entropy catalysts for the oxygen evolution reaction (OER), which plays a pivotal role in renewable energy technologies, and is especially critical for overcoming the kinetic barriers associated with water splitting and metal-air batteries.[43–45] An initial dataset was constructed by systematically varying the catalyst elemental compositions. The synthesis, characterization, and testing of these catalysts were performed on the robotic AI-Chemist experimental platform. Further optimization was achieved through the development of Spectral Generative (SpecGen) model, which generates and predicts the spectra of optimal catalysts. Integrated with synthetic robots, this model harnessed spectroscopic descriptors to drive the autonomous inverse design of senary high-entropy metal-organic hybrid catalysts (Fig. 1a). The SpecGen model comprises three interconnected components: a VAE for extracting and generating spectral features from spectroscopic descriptors, a spectra-to-performance (S2P) model for predicting catalytic overpotential, and a spectra-to-composition (S2C) model for predicting metal composition. The latent space of VAE model was sampled to generate new spectroscopic data, which were then processed by the S2P model to predict their catalytic performance. Catalysts meeting the desired performance criteria were subsequently fed into the S2C model to predict their corresponding compositions.

This process allowed the SpecGen model to generate a new set of high-entropy catalyst candidates with the lowest predicted overpotentials. These catalysts were then synthesized and experimentally analyzed by AI-Chemist (Fig. 1b). Transfer learning was employed to assess the adaptability of AIGC model across different metal and ligand combinations, confirming its potential for broader applications in derivative systems. Our work illustrates the effectiveness of the SpecGen design strategy, which, in combination with the automated experimental platform, shows the potential to significantly advance catalyst design and is anticipated to have a broad impact on materials science as a whole.

Results

The AI-Chemist Executed High-Throughput Synthesis and Spectroscopic Characterization of High-Entropy Catalysts

The AI-chemist automated experimental platform, adapted from our previous work, was instrumental in streamlining the synthesis and testing of high-entropy catalysts, while ensuring precise control over experimental parameters.[46,47] It includes a mobile robotic arm and a stationary six-axis robotic arm that is mounted to a high-throughput characterization station. Full automation is achieved by linking the robotic arms, raw materials dispensing station, stirrer, centrifuge, spectroscopic workstation, and electrochemical workstation to a cloud-based computational server (Fig. 2a). Researchers remotely control the robots and workstations, configuring the modules for all catalyst preparation and analysis steps.

In the synthesis module, various metals are combined in specific ratios to produce high-entropy catalysts. The testing module applies catalyst slurry onto carbon paper substrates using a modified electronic pipette. These samples are then transferred to the electrochemical workstation for OER performance testing. Additionally, the automated system features an autosampler that transfers catalysts to a spectrophotometer for UV-Vis-NIR spectra analysis, completing the entire experimental workflow (Supplementary Fig. S1 and Video S1).

A diverse library of high-entropy catalysts was prepared by systematically varying the ratios of six divalent metals (Co, Ni, Cu, Mg, Cd, Zn) incorporated into a hybrid metal-organic structure with terephthalic acid (Fig. 2b). Using a high-throughput, automated wet-chemistry approach, 462 catalysts were synthesized and characterized (compositions in Supplementary Table S1). Unlike the conventional manual process, which requires about 20 hours per sample, the AI-chemist prepared samples in batches of 40. This enabled the generation of the entire dataset in just 25 days, with an average turnaround time of only 78 minutes per sample, encompassing synthesis, characterization, and electrochemical testing (Supplementary Fig. S2).

Figure 2c shows an overlay of the resulting 462 UV-Vis-NIR absorption spectra, revealing significant variation among the high-entropy catalysts. These spectral differences reflect variations in the catalyst electronic structures, which may influence their catalytic performances. A histogram of the working current density at 10 mA/cm² (η_{10}) measured for the catalysts (Fig. 2d) illustrates the substantial disparity between the best-performing (Exp-451, η_{10} = 324.3 mV) and worst-performing (Exp-103, η_{10} = 465.6 mV) catalysts, highlighting the sensitivity of performance to elemental composition.

High-angle annular dark-field scanning transmission electron microscopy (HAADF-STEM) images in Fig. 2e confirmed the amorphous nature of the as-prepared materials, as evidenced by the loose halo in the selected area electron diffraction (SAED) patterns. This observation was further corroborated by X-ray diffraction (XRD) results (Supplementary Fig. S3). Despite the amorphous structure, energy-

dispersive X-ray (EDX) mapping revealed a high degree of configurational entropy, indicating uniform elemental distribution. The amorphous nature of these catalysts challenges the conventional structure-property relationship paradigm, suggesting that traditional forward predictive models may be insufficient for designing high-entropy catalysts.

Optimizing Catalyst Formulations via a Generative AI Model with Spectroscopic Descriptors

To identify catalyst metal compositions that optimize performance, we developed a ML framework consisting of three modules. Each module was independently trained using the 462 experimental UV-Vis-NIR spectra collected by AI-chemist. The dataset was independently split into 80% for training and 20% for testing. The VAE module was trained to extract latent spectral features from the experimental data (Supplementary Note S1). It achieved a Spearman correlation of 0.996 between the experimental spectra and those reconstructed from the VAE latent space (Supplementary Fig. S4). The S2C module, a one-dimensional convolutional neural network (CNN), was trained to predict catalyst metal composition from the spectroscopic descriptors, showing excellent predictive accuracy on an independent test set (Fig. 3a). A second CNN module, S2P, was then trained to predict OER overpotentials as a measure of catalyst performance, yielding a high correlation of 0.917 between predicted and experimental overpotentials. The mean absolute error (MAE) of these overpotential measurements was 10.8 mV (Fig. 3b).

The latent space of the VAE model was randomly sampled 10,000,000 times to generate a new dataset of synthetic spectra. Using the S2P model to predict the catalysts OER performances, the 20 spectra with the lowest predicted η_{10} were selected (Fig. 4a). The corresponding metal compositions for these 20 spectra were predicted using the S2C model and were synthesized and characterized by AI-Chemist. Of these, 40% (8 out of 20) exhibited superior performance (i.e. lower η_{10}) compared to the best previously obtained result, Exp-451 (Fig. 4b and Supplementary Table S2). The best-performing catalyst, with composition of $Co_{0.4175}Ni_{0.0058}Cu_{0.3411}Mg_{0.1310}Cd_{0.0753}Zn_{0.0294}$, achieved an η_{10} value of 292.3 mV, representing a significant 32 mV reduction relative to Exp-451. It is noteworthy that the composition of this optimized catalyst differed significantly from the previously identified local optimum, as illustrated by the Kiviat plots in Fig. 4c.

In contrast, when 20 additional spectra were randomly generated using the VAE model and their corresponding compositions were predicted using the S2C model, none of the resulting catalysts had lower experimentally measured overpotentials at 10 mA/cm² than Exp-451 (Supplementary Table S3). We also explored a traditional forward prediction model, the composition-to-performance (C2P) model, which directly predicts overpotentials from metal compositions without incorporating spectral data. This model was trained similarly to the S2C and S2P models using the same dataset of 462 catalysts. A fine-grained grid search, varying metal ratios in 2% increments, was used to explore the entire catalyst compositional space. The η_{10} values predicted for the top 20 catalysts ranged from 330.83 to 368.71 mV

(Supplementary Table S4). None of these catalysts had lower S2P predicted overpotentials than Exp-451.

In sharp contrast to the results obtained with our SpecGen inverse design approach, the best OER catalyst identified by the C2P model had a composition similar to Exp-451. These findings highlight that spectra data provide critical information not captured by metal composition alone. Leveraging this information allows us to transcend the limitations of traditional experimental design and identify new potential global optima, opening up new possibilities for the realistic inverse design of highly efficient catalysts.

Intrinsic OER Activity at Active Sites of Senary High-Entropy Catalysts: A Detailed Analysis

In-situ Raman spectroscopy was used to capture transient active species on both the locally optimal Exp-451 catalyst and the SpecGen-optimized catalyst during the OER process, with a focus on key intermediate species (Supplementary Fig. S5).[48,49] At 1.2 V, no adsorbed species were detected on any catalyst-coated substrates. However, as the potential increased to 1.8 V, vibrational modes corresponding to $\delta_{(M^{3+}-O)}$ and $\nu_{(M^{3+}-O)}$ gradually emerged, indicating the formation of M-OOH intermediates, consistent with the sequential steps of OER mechanism. Remarkably, the SpecGen-optimized catalyst exhibited the formation of OOH at a lower starting potential of 1.3 V, suggesting that the tailored metal composition facilitated the creation of an active surface layer and improved OER performance. The emergence and intensification of doublet peaks at 445 and 561 cm^{-1} above 1.4 V signaled the formation of amorphous hydroperoxy species on both catalysts (Fig. 2e and Supplementary Fig. S6). The higher intensity of these peaks for the SpecGen-optimized catalyst indicated enhanced OER activity, in agreement with the linear sweep voltammetry (LSV) results shown in Fig. 4d.

Comprehensive electrochemical analyses were conducted to understand the enhanced performance of the SpecGen-optimized catalyst. The Tafel slope, derived from LSV data, was found to be significantly lower for the SpecGen-optimized catalyst compared to Exp-451, indicating faster kinetics for OER process (Fig. 4e). Electrochemical impedance spectroscopy (EIS) measurements further supported this, revealing a lower charge transfer resistance for the SpecGen-optimized catalyst, suggesting more efficient charge transfer at the electrode-electrolyte interface (Supplementary Fig. S7). Electrochemically active surface area (ECSA) measurements, shown in Fig. 4f and Supplementary Fig. S8, derived from double-layer capacitance analysis, demonstrated substantially higher intrinsic activity for the SpecGen-optimized catalyst. This reflects improved interfacial contact between the catalyst surface and H_2O molecules, enhancing mass transport and accelerating O_2 bubble formation.

To assess long-term durability, a stress test was performed on the SpecGen-optimized catalyst under operando conditions. It displayed superior stability, maintaining a constant current density of 10 mA/cm^2 in 1 M KOH for over 1500 hours without significant degradation (Fig. 4g). Additionally, the average

Faradaic efficiency exceeded 99% and 98% at current densities of 10 and 50 mA/cm², respectively (Supplementary Fig. S9). These results suggest that the remarkable performance of the SpecGen-optimized catalyst would transfer well to real-world applications.

Validating Transfer Learning in the Spectroscopic Generative Model for Predicting Derivative Systems

To evaluate the generalizability of SpecGen model, we conducted a comprehensive set of transfer learning analyses. Four different analyses were performed: two involved substituting the terephthalic acid organic ligand with either 1,3,5-benzenetricarboxylic acid or 2-aminoterephthalic acid, and two others involved retaining the original terephthalic ligand but substituting the Cd metal center with Mn or the Mg metal center with Fe. For each analysis, a library of 126 catalysts was generated by systematically varying the metal ratios. These catalysts were efficiently synthesized and characterized using AI-Chemist (Supplementary Table S5). The spectral datasets for each transfer learning analysis were split, with 80% used for model training and 20% for testing. Only S2C model was fine-tuned based on the new data. The top 20 spectra from previous generation were then directly applied to the fine-tuned S2C model, and their metal compositions were predicted using the fine-tuned S2C model. These catalysts were then synthesized and characterized by AI-Chemist.

The results showed strong transferability of the SpecGen model when substituting the terephthalic ligand with 1,3,5-benzenetricarboxylic acid or substituting Cd with Mn, yielding average correlation coefficients of 0.830 and 0.794, respectively (Fig. 5 and Supplementary Fig. S10-S11). In the 1,3,5-benzenetricarboxylic acid derivative system, 8 of the top 20 predicted catalysts demonstrated improved OER activity compared to the original 126 catalysts (Supplementary Fig. S12 and Table S6). In the Mn-substituted system, 13 out of the top 20 predicted catalysts showed enhanced performance relative to the original set (Supplementary Fig. S13 and Table S7).

We attribute the success of these transfer learning models to the use of spectroscopic descriptors, which capture the chemical microenvironment of the active sites in catalysts. These descriptors, unlike structural ones, are less sensitive to the specific identity of the ligands or metals and can therefore generalize across different systems. This finding suggests that catalysts with similar spectroscopic features may share common catalytic properties, allowing for the design of new catalysts by targeting specific spectral features rather than conducting exhaustive experimental studies on each system.

While the SpecGen exhibited strong transferability in some cases, its performance declined significantly when confronted with drastic changes to the chemical microenvironment. Specifically, replacing terephthalic acid with 2-aminoterephthalic acid or replacing Mg with Fe severely impacted SpecGen transfer learning capabilities. For the 2-aminoterephthalic acid and Fe derivative systems, the average correlation coefficients of the fine-tuned S2C models dropped markedly to 0.753 and 0.655, respectively (Supplementary Fig. S14-S15). Additionally, for both systems, the top 20 catalysts predicted by the

SpecGen model failed to identify better-performing catalysts (Supplementary Fig. S16-S17 and Tables S8-S9).

We attribute this to several factors: Asymmetric ligand substitution can disrupt the structural symmetry of the catalyst, which in turn alters its electronic properties and catalytic activity. Furthermore, metals like Fe^{2+} are prone to oxidation, which can modify the electronic structure of catalytic sites. Lastly, substantial changes in the intensity and direction of ligand-to-metal charge transfer (LMCT) can significantly affect the electronic states of catalytic sites, undermining the fundamental correlations already learned by the model.

Conclusion

Our study highlights the superiority of a spectroscopic descriptor-driven inverse design approach for developing high-performance catalysts, as demonstrated for OER catalysts. We integrated a robotic platform with the SpecGen model, automating the discovery of optimal high-entropy catalysts. By correlating spectral features with catalyst performance and composition, our model enables the rapid identification of the promising formulations, surpassing the efficacy of trial-and-error methods. The generative model's transferability, facilitated by spectral descriptors, enables the design of catalysts in derivative systems. This integrated approach—combining artificial intelligence, robotics, and spectroscopic descriptors—accelerates the inverse design process, advancing the development of high-performance catalysts with tailored functionalities.

Future research could focus on enhancing the robustness of generative models by integrating a wider range of spectroscopic descriptors (e.g., absorption, emission, scattering, vibrational, rotational, and spin) and utilizing advanced machine learning algorithms for spectral feature extraction. This would help capture the complex relationships between material composition, structure, electronic properties, and catalytic performance.

Methods

Materials. Potassium hydroxide (KOH, 99.9%), metal acetates (> 99%), anhydrous ethanol, and 5 wt% Nafion 117 solution were purchased from Sigma-Aldrich. 1,4-benzenedicarboxylic acid, 2-aminobenzene-1,4-dicarboxylic acid, and 1,3,5-benzenetricarboxylic acid were obtained from Shanghai Aladdin Bio-Chem Technology Co., LTD. Dimethylformamide (DMF) used to prepare the metal feedstock solution was purchased from Acros Organics. A graphite rod counter electrode and a Ag/AgCl reference electrode in saturated potassium chloride were obtained from CH Instruments. Deionized water (18.2 MΩ cm-1) for the aqueous electrolyte was prepared using a Milli-Q EQ 7000 ultrapure water purification system.

Robotic experiment procedure. A high-throughput synthesis protocol was employed for the preparation of high-entropy catalysts. Metal acetate precursors and a ligand solution were preloaded into a liquid dispensing station. A robotic arm transferred racks containing empty vials from a starting position to the

liquid dispensing station, where a predefined recipe was executed to sequentially add metal precursors and the ligand. The vials were then transferred to the magnetic stirrer for a 12-hour reaction. Solid-liquid separation was achieved using a centrifuge at 4000 rpm for 5 min. The supernatant was removed, and the catalyst precipitate was retained. The solid product was dried and redispersed in a 10 mL ethanol/Nafion mixture. The resulting catalyst suspension was then transferred onto carbon paper using a high-throughput pipetting platform. The prepared working electrodes were subsequently moved to an electrolysis cell for OER performance evaluation using a specialized soft gripper. In parallel, a portion of the catalyst was loaded onto a tray of amorphous substrate for subsequent X-ray diffraction characterization, which were obtained using a Miniflex X-ray diffractometer (Rigaku, Japan) with Cu Kα radiation (λ = 1.540598 nm). The XRD data were collected in the 2θ range of 10° to 70° with a step of 0.1°. Another portion of the catalyst dispersion was introduced into a UV-Vis Spectrophotometer (UV-2600i/2700i) by an automatic sampler (ASC-5) for spectra measurements. The wavelength range extended from 280 to 1000 nm, with a step resolution of 1 nm, and the upper threshold for the maximum absorbance was set at 4 OD.

Electrochemical property measurements. Electrochemical measurements were conducted using a CHI760E workstation in a standard three-electrode configuration. The high-entropy catalyst served as the working electrode, with graphite and Ag/AgCl as counter and reference electrodes, respectively. OER activity was assessed in 1 M KOH, with potentials calibrated to reversible hydrogen electrode (RHE) following the formula $E_{RHE} = E_{Ag/AgCl}+0.0591\times pH + 0.197$ V. Catalyst ink was prepared by dispersing the catalyst in a 10 mL ethanol/Nafion mixture, and then drop-casting 150 μL onto 1.5×1.5 cm^2 carbon paper. Electrochemical characterization included CV activation, LSV, EIS, and chronoamperometry. CV activation involved 40 cycles from 1.0 to 1.5 V vs. RHE at scanning rate of 50 mV s^{-1}. Then, LSV was performed from 1.0 to 1.8 V vs. RHE at 5 mV s^{-1} and neither iR-compensation nor background current correction was applied. EIS measurements were conducted at 300 mV overpotential spanning the range from 100 kHz to 0.1 Hz. ECSA was determined from CVs in the non-Faradaic region (1.05–1.15 V vs. RHE) at varying scan rates. Chronoamperometry was performed at a constant working current density of 10 mA/cm^2 in the standard three-electrode configuration.

Identification of transient electrochemically active species. In-situ Raman spectroscopy was performed using a LabRAM HR Evolution confocal Raman microscope coupled with a CHI-660 electrochemical workstation. A home-built single-compartment PTFE electrochemical cell equipped with a circular quartz optical window was employed for the measurements. The working electrode was a 1.5 cm × 1.5 cm carbon paper coated with the catalyst, while a Pt foil and a KCl-saturated Ag/AgCl electrode served as the counter and reference electrodes, respectively. A 1 M KOH solution, saturated with air for 30 minutes, was used as the electrolyte. Prior to the experiments, the instrument was calibrated using a silicon wafer (520.5 cm^{-1}). A 532 nm laser with a power of 5% was focused onto the working electrode surface through a 50× objective lens. Raman spectra were collected in the range of 100–1200 cm^{-1} using a 600 lines/mm grating after stabilization with different bias applied to the working electrode. Each spectrum was acquired with an accumulation time of 10 seconds and 10 accumulations.

Neural network architecture. A one-dimensional convolutional neural network (CNN)[50] was developed using PyTorch library[51] to predict the metal composition of catalysts. This model, referred to as the S2C Model, consists of multiple sub-models, each dedicated to predicting the composition of a single metal element and all of them share the same structure. The final output is obtained by applying sum normalization to the predictions from each sub-model, thereby yielding the composition of all metal elements. Each sub-model takes one-dimensional spectral descriptors as input, extracting features through three one-dimensional convolutional layers, batch normalization,[52] and one-dimensional max pooling. The extracted features are then flattened and passed through fully connected layers to predict the metal composition. The ReLU function was employed as the activation function, and the MAE was used as the loss function. To optimize the model parameters, the Adam optimization algorithm[53] was utilized with an initial learning rate of 1×10^{-3}, and a learning rate decay strategy was applied. The dataset was split into 80% for training and 20% for testing, with each sub-model being trained independently. The model for predicting the catalytic overpotentials, designated as the S2P Model, exhibits a structural parallelism with the sub-models employed in the S2C Model for forecasting individual metal compositions. Similar to the S2C Model, the S2P Model is established upon a one-dimensional CNN and adheres to the same dataset partitioning strategy as in the training process of S2C model.

Additionally, a Variational Autoencoder (VAE) model was constructed using PyTorch. The model comprises an encoder and a decoder. The encoder accepts one-dimensional spectral descriptors as input, extracting features through the application of one-dimensional convolutional layers, batch normalization, and max pooling. Subsequently, the extracted features are flattened and passed into two separate fully connected layers, which are utilized to predict the mean and log variance of the latent variables, respectively. The parameterization trick is employed to sample latent variables from the distribution defined by the predicted mean and variance. In short, the decoder receives the aforementioned latent variables and reconstructs the spectra through two fully connected layers. The ReLU function was employed as the activation function, and the model loss function is a combination of MAE and KL divergence. The model parameters are optimized using the Adam optimization algorithm with an initial learning rate of 1×10^{-3}, along with a learning rate decay strategy. The dataset was divided in accordance with the same methodology employed for training the S2C model.

For transfer learning, the training set comprised 80% of the whole dataset, while the remaining 20% constituted the testing set. From the very beginning, all layers were frozen with the exception of the final layer, and the model was trained with an initial learning rate of 1×10^{-3}. Subsequently, all layers were unfrozen, and the initial learning rate was adjusted to 1×10^{-4} for fine-tuning.

The C2P model takes the metal compositions as input, extracting features through two fully connected layers to predict the catalytic overpotentials. Each fully connected layer consisted of 128 neurons. A dropout with a rate of 0.25 was used after each fully connected layer during training. The ReLU function was employed as the activation function, and the MAE was used as the loss function. To optimize the

model parameters, the Adam optimization algorithm was utilized with an initial learning rate of 1×10^{-3}, and a learning rate decay strategy was applied. The dataset was split into 80% for training and 20% for testing.

Declarations

Competing interests

The authors declare no competing interests.

Author contributions

[#]D.Z., R.Y., and Z.J. contributed equally to this work.

Acknowledgements

Q.Z. acknowledges the National Key R&D Program of China (2024YFB3817302) and National Natural Science Foundation of China (22103076) and Anhui Provincial Natural Science Foundation (2108085QB63) and Henan Provincial Natural Science Foundation (242300421138) and Joint Fund of Henan Province Science and Technology R&D Program (235200810107) and USTC Research Funds of the Double First-Class Initiative (YD9990002032). J.J. acknowledge the Strategic Priority Research Program of the Chinese Academy of Sciences (XDB0450302) and the National Natural Science Foundation of China (22025304, 22033007) and the CAS Project for Young Scientists in Basic Research (YSBR-005). Y.H. acknowledges the National Natural Science Foundation of China (22303091) and the Fundamental Research Funds for the Central Universities (WK9990000130) and the National Key Research and Development Program of China (2023YFA1508200). We also gratefully acknowledge the USTC Center for Micro- and Nanoscale Research and Fabrication for providing experimental resources and the USTC supercomputing center, and Hefei Advanced Computing Center for providing computational resources.

Code availability

All the code used for training the SpecGen Model for OER performance and composition prediction with theoretical data and robot-driven spectroscopic and electrochemical data is available on GitHub at https://github.com/Tony935/SpecGen.

Data availability

The authors declare that the data supporting the findings of this study are available and provided within the paper and its Supplementary Information files.

References

1. Freeze, J. G., Kelly, H. R. & Batista, V. S. Search for Catalysts by Inverse Design: Artificial Intelligence, Mountain Climbers, and Alchemists. Chem. Rev. 119, 6595–6612 (2019).
2. Liu, H. *et al.* Inverse design of a pyrochlore lattice of DNA origami through model-driven experiments. Science 384, 776–781 (2024).
3. Yao, Z. *et al.* Inverse design of nanoporous crystalline reticular materials with deep generative models. Nat. Mach. Intell. 3, 76–86 (2021).
4. Wang, K. *et al.* Synergy of cations in high entropy oxide lithium ion battery anode. Nat. Commun. 14, 1487 (2023).
5. Liu, M. *et al.* Interfacial electronic structure engineering on molybdenum sulfide for robust dual-pH hydrogen evolution. Nat. Commun. 12, 5260 (2021).
6. Ren, J. *et al.* The Electron-Rich and Nucleophilic N-Heterocyclic Imines on Metal Surfaces: Binding Modes and Interfacial Charge Transfer. J. Am. Chem. Soc. 146, 7288–7294 (2024).
7. Mou, T. *et al.* Bridging the complexity gap in computational heterogeneous catalysis with machine learning. Nat. Catal. 6, 122–136 (2023).
8. Hitt, J. L. *et al.* A high throughput optical method for studying compositional effects in electrocatalysts for CO_2 reduction. Nat. Commun. 12, 1114 (2021).
9. Kim, M. *et al.* Acidic Hydrogen Evolution Electrocatalysis at High-Entropy Alloys Correlates with its Composition-Dependent Potential of Zero Charge. Angew. Chemie Int. Ed. 62, e202310069 (2023).
10. Xu, W., Diesen, E., He, T., Reuter, K. & Margraf, J. T. Discovering High Entropy Alloy Electrocatalysts in Vast Composition Spaces with Multiobjective Optimization. J. Am. Chem. Soc. 146, 7698–7707 (2024).
11. Yao, Y. *et al.* High-throughput, combinatorial synthesis of multimetallic nanoclusters. *Proc. Natl. Acad. Sci.* 117, 6316–6322 (2020).
12. Löffler, T., Ludwig, A., Rossmeisl, J. & Schuhmann, W. What Makes High-Entropy Alloys Exceptional Electrocatalysts? Angew. Chemie Int. Ed. 60, 26894–26903 (2021).
13. Esterhuizen, J. A., Goldsmith, B. R. & Linic, S. Interpretable machine learning for knowledge generation in heterogeneous catalysis. Nat. Catal. 5, 175–184 (2022).
14. Yao, Y. *et al.* High-entropy nanoparticles: Synthesis-structure-property relationships and data-driven discovery. Science 376, eabn3103 (2023).
15. Mou, L.-H., Han, T., Smith, P. E. S., Sharman, E. & Jiang, J. Machine Learning Descriptors for Data-Driven Catalysis Study. Adv. Sci. 10, 2301020 (2023).
16. Schweidler, S. *et al.* High-entropy materials for energy and electronic applications. Nat. Rev. Mater. 9, 266–281 (2024).

17. Pollice, R. *et al.* Data-Driven Strategies for Accelerated Materials Design. Acc. Chem. Res. 54, 849–860 (2021).
18. Xie, Y. *et al.* Inverse design of chiral functional films by a robotic AI-guided system. Nat. Commun. 14, 6177 (2023).
19. Ma, W., Cheng, F., Xu, Y., Wen, Q. & Liu, Y. Probabilistic Representation and Inverse Design of Metamaterials Based on a Deep Generative Model with Semi-Supervised Learning Strategy. Adv. Mater. 31, 1901111 (2019).
20. Sanchez-Lengeling, B. & Aspuru-Guzik, A. Inverse molecular design using machine learning: Generative models for matter engineering. Science 361, 360–365 (2018).
21. Anstine, D. M. & Isayev, O. Generative Models as an Emerging Paradigm in the Chemical Sciences. J. Am. Chem. Soc. 145, 8736–8750 (2023).
22. Peng, J. *et al.* Human- and machine-centred designs of molecules and materials for sustainability and decarbonization. Nat. Rev. Mater. 7, 991–1009 (2022).
23. Gebauer, N. W. A., Gastegger, M., Hessmann, S. S. P., Müller, K.-R. & Schütt, K. T. Inverse design of 3d molecular structures with conditional generative neural networks. Nat. Commun. 13, 973 (2022).
24. Kingma, D. P. Auto-encoding variational bayes. *arXiv Prepr. arXiv1312.6114* (2013).
25. Winter, R. *et al.* Efficient multi-objective molecular optimization in a continuous latent space. Chem. Sci. 10, 8016–8024 (2019).
26. Kalinin, S. V, Dyck, O., Jesse, S. & Ziatdinov, M. Exploring order parameters and dynamic processes in disordered systems via variational autoencoders. Sci. Adv. 7, eabd5084 (2021).
27. Yang, T. *et al.* Catalytic Structure Design by AI Generating with Spectroscopic Descriptors. J. Am. Chem. Soc. 145, 26817–26823 (2023).
28. Du, W. *et al.* Spectroscopy-Guided Deep Learning Predicts Solid–Liquid Surface Adsorbate Properties in Unseen Solvents. J. Am. Chem. Soc. 146, 811–823 (2024).
29. Trummer, D. *et al.* Deciphering the Phillips Catalyst by Orbital Analysis and Supervised Machine Learning from Cr Pre-edge XANES of Molecular Libraries. J. Am. Chem. Soc. 143, 7326–7341 (2021).
30. Yokota, Y., Wong, R. A., Hong, M., Hayazawa, N. & Kim, Y. Monatomic Iodine Dielectric Layer for Multimodal Optical Spectroscopy of Dye Molecules on Metal Surfaces. J. Am. Chem. Soc. 143, 15205–15214 (2021).
31. Dodo, K., Fujita, K. & Sodeoka, M. Raman Spectroscopy for Chemical Biology Research. J. Am. Chem. Soc. 144, 19651–19667 (2022).
32. Bols, M. L. *et al.* In Situ UV–Vis–NIR Absorption Spectroscopy and Catalysis. Chem. Rev. 124, 2352–2418 (2024).
33. Jana, M. K. *et al.* Structural descriptor for enhanced spin-splitting in 2D hybrid perovskites. Nat. Commun. 12, 4982 (2021).

34. Han, X.-B., Jing, C.-Q., Zu, H.-Y. & Zhang, W. Structural Descriptors to Correlate Pb Ion Displacement and Broadband Emission in 2D Halide Perovskites. J. Am. Chem. Soc. 144, 18595–18606 (2022).
35. Han, Z. *et al.* Machine-learning-assisted design of a binary descriptor to decipher electronic and structural effects on sulfur reduction kinetics. Nat. Catal. 6, 1073–1086 (2023).
36. Hueffel, J. A. *et al.* Accelerated dinuclear palladium catalyst identification through unsupervised machine learning. Science 374, 1134–1140 (2021).
37. Artrith, N. *et al.* Best practices in machine learning for chemistry. Nat. Chem. 13, 505–508 (2021).
38. Yao, Z. *et al.* Machine learning for a sustainable energy future. Nat. Rev. Mater. 8, 202–215 (2023).
39. Burger, B. *et al.* A mobile robotic chemist. Nature 583, 237–241 (2020).
40. Rohrbach, S. *et al.* Digitization and validation of a chemical synthesis literature database in the ChemPU. Science 377, 172–180 (2022).
41. Angello, N. H. *et al.* Closed-loop optimization of general reaction conditions for heteroaryl Suzuki-Miyaura coupling. Science 378, 399–405 (2022).
42. Angello, N. H. *et al.* Closed-loop transfer enables artificial intelligence to yield chemical knowledge. Nature (2024) doi:10.1038/s41586-024-07892-1.
43. Kang, J. *et al.* Valence oscillation and dynamic active sites in monolayer NiCo hydroxides for water oxidation. Nat. Catal. 4, 1050–1058 (2021).
44. Wu, Z.-Y. *et al.* Non-iridium-based electrocatalyst for durable acidic oxygen evolution reaction in proton exchange membrane water electrolysis. Nat. Mater. 22, 100–108 (2023).
45. Li, Z. *et al.* Seed-assisted formation of NiFe anode catalysts for anion exchange membrane water electrolysis at industrial-scale current density. Nat. Catal. (2024) doi:10.1038/s41929-024-01209-1.
46. Zhu, Q. *et al.* An all-round AI-Chemist with a scientific mind. Natl. Sci. Rev. 9, nwac190 (2022).
47. Zhu, Q. *et al.* Automated synthesis of oxygen-producing catalysts from Martian meteorites by a robotic AI chemist. Nat. Synth. 3, 319–328 (2024).
48. Louie, M. W. & Bell, A. T. An Investigation of Thin-Film Ni–Fe Oxide Catalysts for the Electrochemical Evolution of Oxygen. J. Am. Chem. Soc. 135, 12329–12337 (2013).
49. Singha Roy, S., Nagappan, S., Satheesan, A. K., Karmakar, A. & Kundu, S. Surface-Enhanced Raman Scattering Coupled with In Situ Raman Spectroscopy for the Detection of the OER Mechanism: A Mini-Review. J. Phys. Chem. C 128, 13634–13650 (2024).
50. Krizhevsky, A., Sutskever, I. & Hinton, G. E. Imagenet classification with deep convolutional neural networks. Commun. ACM 60, 84–90 (2017).
51. Paszke, A. *et al.* Pytorch: An imperative style, high-performance deep learning library. Adv. Neural Inf. Process. Syst. 32, (2019).
52. Ioffe, S. Batch normalization: Accelerating deep network training by reducing internal covariate shift. *arXiv Prepr. arXiv1502.03167* (2015).
53. Kingma, D. P. Adam: A method for stochastic optimization. *arXiv Prepr. arXiv1412.6980* (2014).

Figures

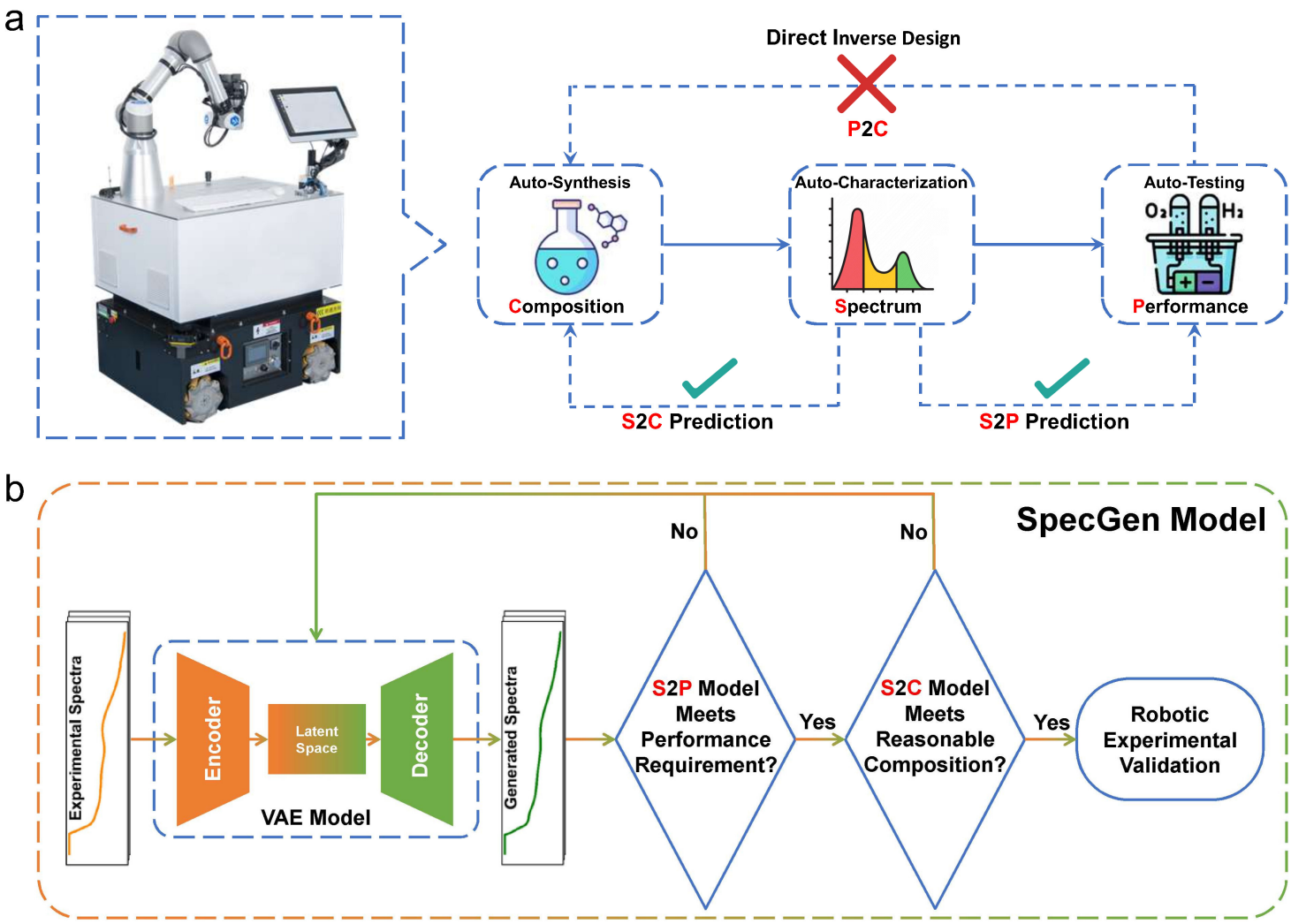


Figure 1

Schematic of the workflow for inverse design of high-entropy catalysts that enabled by a SpecGen model and robotic platform. (a) A dataset of high-entropy catalysts, including their compositions, spectra, and measured OER performances, is obtained using AI-Chemist (left panel). From the resulting spectral data, the spectra-to-performance (S2P) model is trained to predict catalytic overpotential, while the spectra-to-composition (S2C) model is trained to predict metal composition, bridging the catalysts compositions and performances (right panel). (b) The SpecGen model, a generative ML framework comprising VAE, S2P, and S2C components, enables the inverse design of high-entropy catalysts. Latent spectral features are extracted from VAE high-dimensional representation. The S2P model then identifies the best-performing catalyst candidates based on these features, and the S2C model determines their elemental compositions. AI-chemist synthesizes and analyzes the selected candidates, optimizing OER catalyst performance.

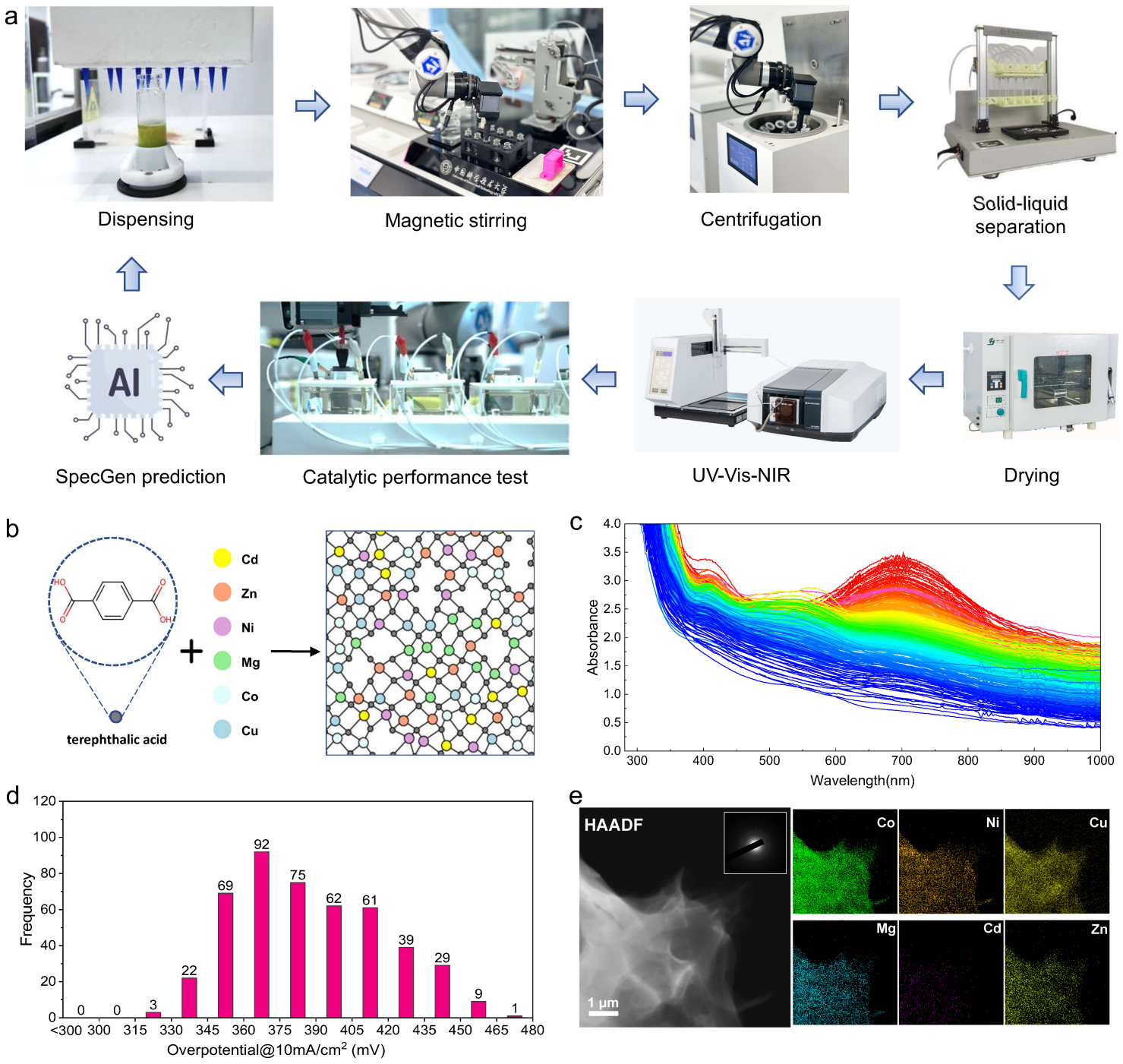


Figure 2

Automated synthesis and characterization of high-entropy catalysts using AI-chemist. (a) Schematic of the AI-chemist experimental workflow integrated with spectroscopic descriptor-based catalyst design, featuring a mobile robot arm collaborated with versatile workstations to automate the synthesis, characterization, and performance testing workflow of high-entropy catalysts. (b) The hybrid structure of the high-entropy catalysts synthesized for OER studies, consisting of terephthalic acid and six metals: Cd, Zn, Ni, Mg, Co and Cu. (c) Overlay of the 462 UV-Vis-NIR spectra collected from experimental samples. (d) Histogram plot of the working current density at 10 mA/cm² (η_{10}) values measured for the

462 catalyst samples. (e) Atomic-resolution HAADF-STEM imaging with EDS elemental mapping of Exp-451, revealing its amorphous structure. The inset shows a selected electron diffractogram.

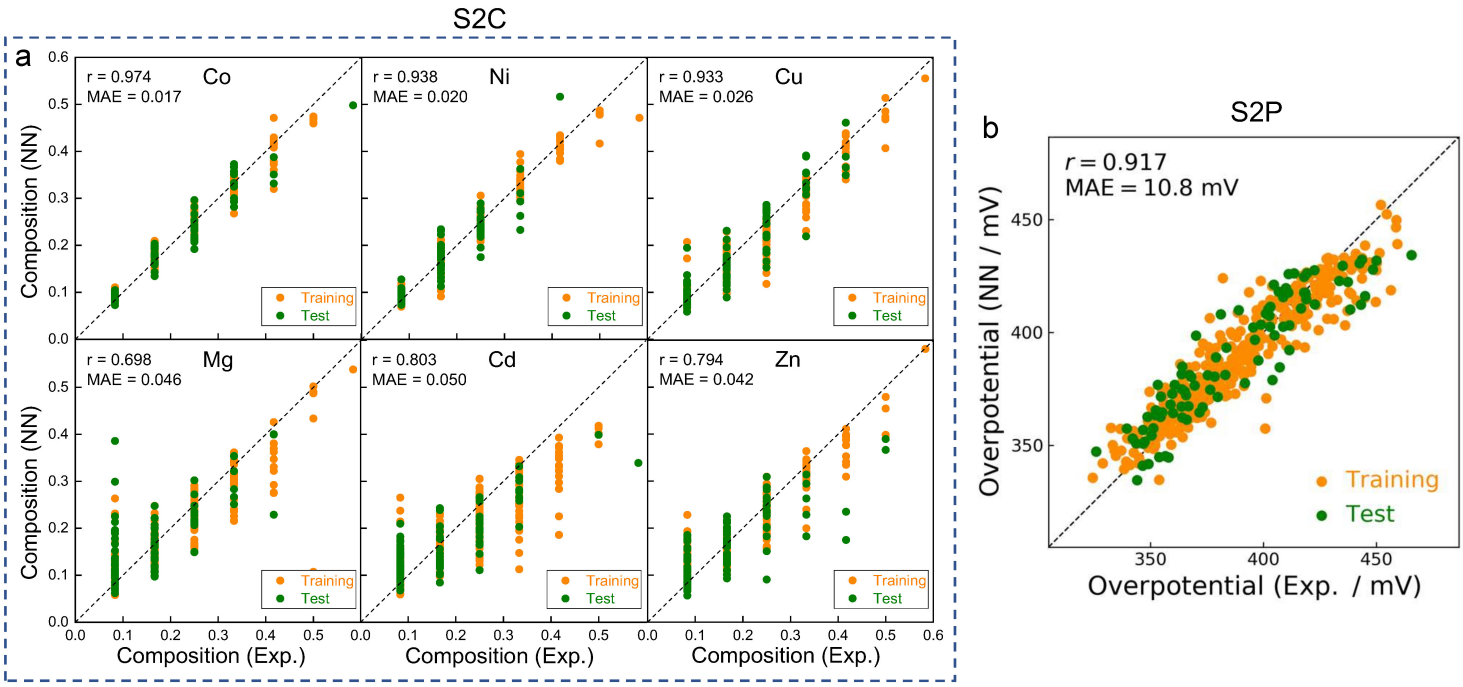


Figure 3

Predictions of metal compositions and overpotentials from spectral data. (a) Correlations between the catalyst synthetic formulations and those predicted by the S2C CNN based on experimental UV-Vis-NIR spectral data. (b) Correlations between experimentally measured catalyst overpotentials and those predicted by the S2P CNN the same spectral data.

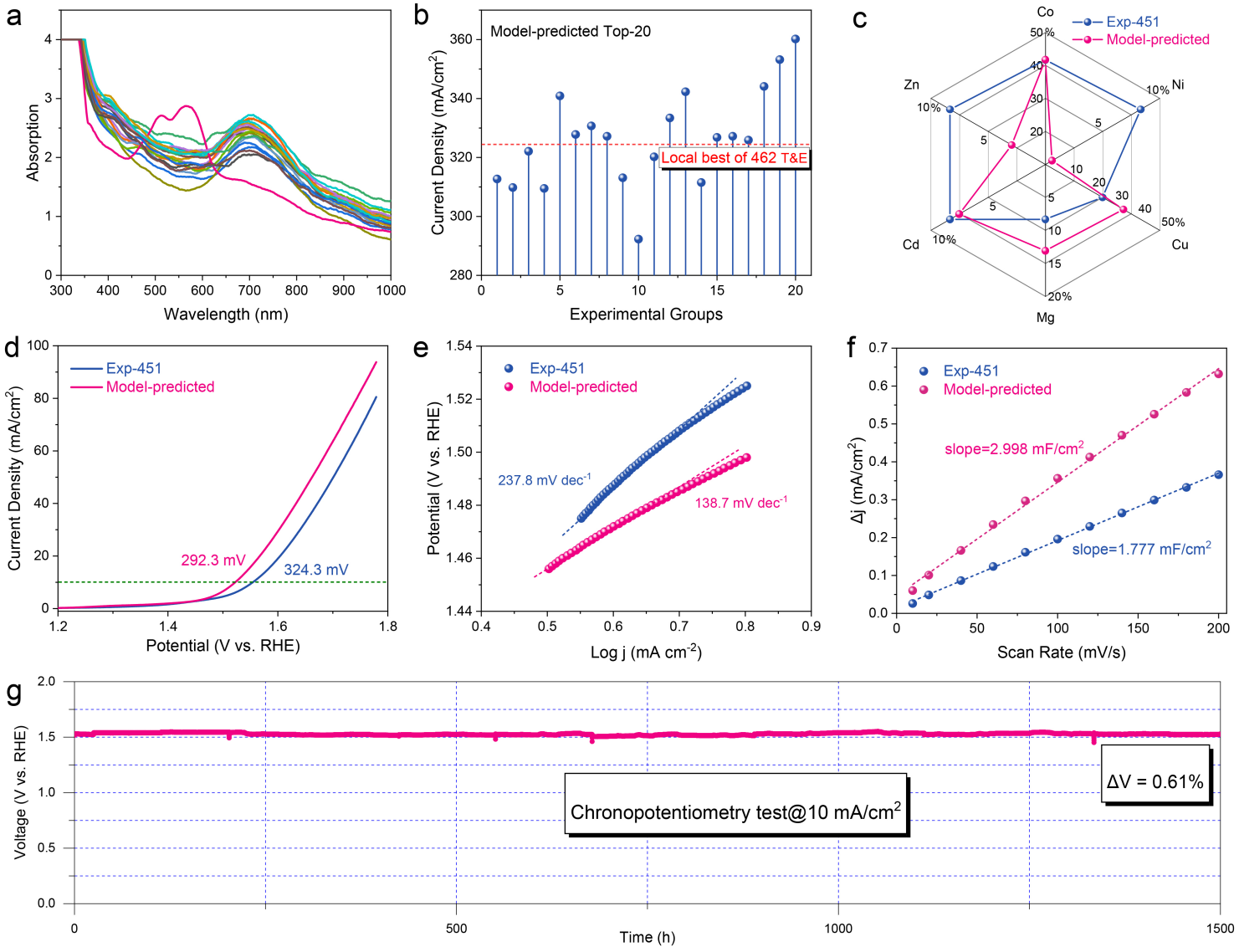


Figure 4

Performance analysis and characterization of the SpecGen-optimized catalyst. (a) Predicted spectra of the top 20 high-entropy catalysts generated by the SpecGen. (b) Experimentally measured overpotentials at 10 mA/cm² for the top 20 high-entropy catalysts generated by SpecGen. (c) Kiviat diagrams comparing the metal compositions of the Exp-451 catalyst with those of the SpecGen-optimized catalyst. (d) Linear sweep voltammetry (LSV) polarization curves at the sweep rate of 5 mV/s without iR correction, and (e) corresponding Tafel plots for both the Exp-451 cand SpecGen-optimized catalysts. (f) Double-layer capacitance, extracted from cyclic voltammetry (CV) data, used to estimate the electrochemically active surface area (ECSA) of the SpecGen-optimized catalyst. (g) Chronoamperometry curve with the SpecGen-optimized catalyst as the working electrode.

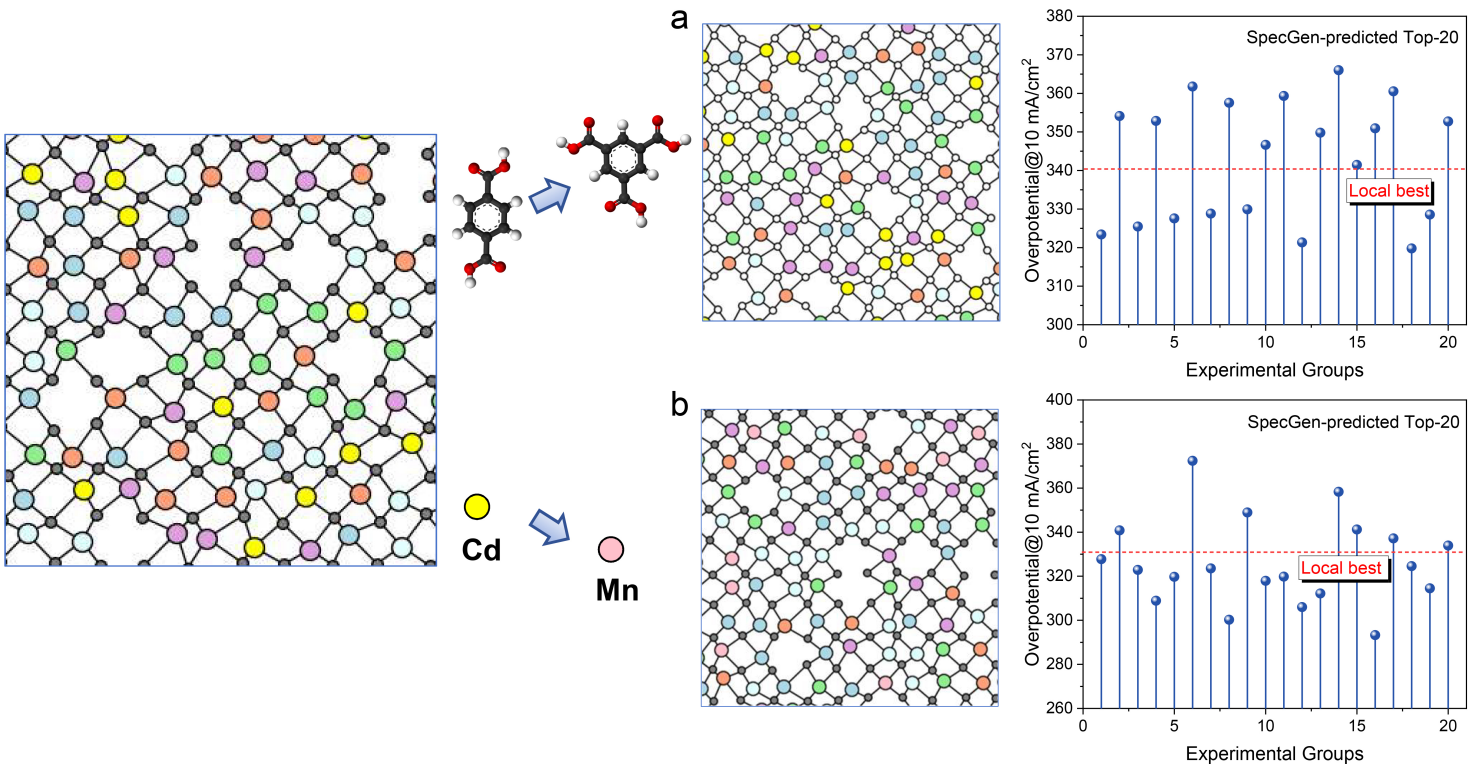


Figure 5

SpecGen transfer learning for derivative metal-organic hybrid catalyst systems. As depicted in the schematic diagram, SpecGen transfer learning generated 20 catalyst candidates for (a) the derivative system with 1,3,5-benzenetricarboxylic acid substituted for terephthalic acid, and (b) the derivative system where Mn is substituted for Cd. The plots on the right show the overpotentials at 10 mA/cm² for these catalysts, as experimentally measured by AI-chemist. The red, dashed line, labeled “Local best,” represents the lowest overpotential identified by AI-chemist from an evaluation 126 candidate catalysts prior to the use of transfer learning and subsequent optimization by SpecGen.

Supplementary Files

This is a list of supplementary files associated with this preprint. Click to download.

- SupplementaryInformation241225.docx
- SupplementaryVideoS1.mp4